Structures 60 (2024) 105886

Contents lists available at ScienceDirect

Structures

journal homepage: www.elsevier.com/locate/structures

Numerical study of combined seismic and aerodynamic loads on wind turbine support structures by coupled and uncoupled approaches

Takeshi Ishihara [a], Yoshihisa Iida [a], Lilin Wang [b,*]

[a] Department of Civil Engineering, School of Engineering, The University of Tokyo, 7-3-1, Hongo, Bunkyo-ku, Tokyo, Japan
[b] Ocean College, Zhejiang University, Zhoushan 316021, PR China

ARTICLE INFO

Keywords:
Wind turbine support structures
Seismic and aerodynamic loads
Misalignment effect
Vector sum
SRSS

ABSTRACT

In this study, the dynamic loads on the wind turbine support structures caused by the combined wind and earthquake are investigated by means of the coupled and uncoupled analysis approaches. A series of numerical models are prepared for a 2.4 MW gravity foundation supported wind turbine including the aero-elastic model, the finite element model, the generation of earthquake inputs and the parameters in the sway-rocking model. The standard lumped mass model with a lumped dashpot at the hub height show good agreement with the aero-elastic model in terms of the modal frequencies and modal shapes. The combined seismic and aerodynamic loads are then investigated using the coupled analyses for various operational scenarios including normal operation, emergency stop and parked condition, in which effects of the wind and earthquake misalignment are considered. When the misalignment equals to 0 degree, the emergency stop yields the maximum tower base moment while when the misalignment reaches 90 degree, the normal operation outputs the maximum loads. The uncoupled analysis approach becomes appealing since it can reduce computational costs significantly and be simper for civil engineers involved in site specific permitting. A series of uncoupled analyses are then performed to investigate the rules to combine the seismic and aerodynamic loads. The vector sum method for the normal operation and parked condition and the SRSS method for the emergency stop are proposed to combine the seismic and aerodynamic loads in the uncoupled analysis approach. The proposed combination criteria show reasonable agreement with the coupled analysis approach.

1. Introduction

The rapid growth of installation of wind farms in seismically active regions enlightens the necessity to consider wind and seismic actions simultaneously when designing the wind turbines. As required by IEC 61400–1 [1], the ground acceleration shall be evaluated for a 475-year return period and the earthquake loads shall be superposed with the operational loads that shall be the largest of a) mean loads during normal power production determined at the rated wind speed V_r, b) loads during emergency stop at rated wind speed V_r, and c) loads during idling or parked condition at no wind and the cut-out wind speed V_{out}. Questions arises that which operational scenario yields the largest operational load. In addition, IEC 61400–1 [1] suggests that the seismic load evaluation may be carried out through response spectrum methods, in which case the operational load is added using the SRSS (square-root-sum-of-squares) or equivalent load combination arising from the seismic loading. It is doubted whether the combination criterion of SRSS suits for all operational scenarios.

Regarding to the seismic consideration in the design of wind turbines, a great many researches have been conducted in the past decades, which can be categorized as those summarized in the comprehensive review by Katsanos et al. [2] and the later publications(Asareh et al. [3], Katsanos et al. [4], Yang et al. [5], Santangelo et al. [6], Avossa et al. [7], Mo et al. [8], Santangelo et al. [9], Failla et al. [10], Zuo et al. [11], Wang et al. [12], Ju and Huang [13], Fan et al. [14], Zuo et al. [15], Risi et al. [16], Kaynia [17], Campo and Pozos-Estrada 2020 [18], Kitahara and Ishihara [19], Wang and Ishihara [20]). Among these publications, some researches (e.g. [16,17,19,20]) investigated some specific aspects of the seismic responses of wind turbine support structures by means of the finite element (FE) model,while other researches (e.g. [3–15,18]) focused on the responses of wind turbines under multi-hazards (e.g. wind, wave or earthquake) by means of the aeroelastic model, the FE model or both aeroelastic and FE models. To support the real design of wind turbine, our attention is paid to the researches that focused on the

* Corresponding author.
E-mail address: lilin.wang@zju.edu.cn (L. Wang).

https://doi.org/10.1016/j.istruc.2024.105886
Received 10 January 2023; Received in revised form 4 November 2023; Accepted 9 January 2024
Available online 25 January 2024

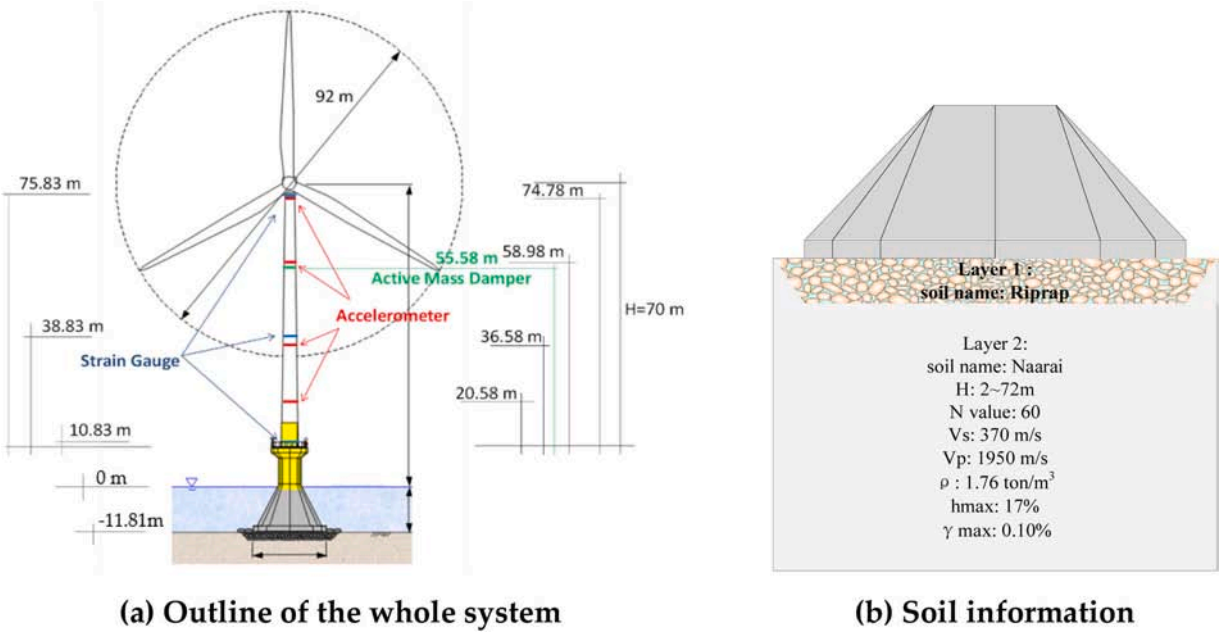

Fig. 1. Choshi wind power plant.

responses of wind turbine under multi-hazards and predicted the aerodynamic loads by the aeroelastic model. A comprehensive review is conducted to define the problems in this study.

As a rigorous approach, the coupled analyses have been performed to predict the combined seismic and aerodynamic loads on wind turbine support structures. More specifically, Witcher [21] performed a series of coupled time-domain analyses to calculate the combined seismic and aerodynamic loads of a 2 MW wind turbine mounted on a 60 m high steel using GH Bladed [22], which is believed to be the pioneering work in this field. Following this line, the coupled analyses were also conducted by Asareh et al. [3] with FAST [23], Katsanos et al. [4] with HAWC2 [24] and Yang et al. [5] with FAST [23]. In addition, the valuable experimental tests on a 65 kW HAWT was carried out by Prowell et al. [25]. Two targets of these coupled analyses can be summarized here. One is to provide the reference data to verify the uncoupled analysis approach, which is explained in the following paragraph. The other is to investigate how the earthquake increases the dynamic loads on wind turbine support structures by considering various operational scenarios including the normal operation, the parked condition and the emergency stop. However, the effect of the angle between wind and earthquake on the combined seismic and aerodynamic loads for different operational scenarios are not clearly investigated. Another issue exists that almost all previous researches focus on the monopile supported wind turbine. Since the soil-structure interaction matters for the seismic loading (see Bazeos et al. [26], Zhao and Maißer [27], Butt and Ishihara [28]), it is necessary to investigate the foundation type on the combined seismic and aerodynamic loads.

As an alternative to the coupled analysis approach, International Standards (e.g. IEC 61400–1 [1]) and Guidelines (e.g. ASCE-AWEA RP2011 [29]) allow to combine two separate analyses for seismic assessment, one with wind only while the other with earthquake only, which is known as the uncoupled analysis approach. The uncoupled analysis approach becomes also popular since the turbine specific codes that directly simulate aerodynamics and seismic loading are often unfamiliar for civil engineers involved in site specific permitting. One major advantage of the uncoupled analysis approach is to significantly reduce the computational costs with respect to the fully coupled analysis approach [6]. The implementation of the uncoupled analyses has been discussed in Witcher [21], Valamanesh and Myers [30], Santangelo et al. [6], Avossa et al. [7], Mo et al. [8], Santangelo et al. [9] and Failla et al. [10]. The effect of aerodynamic damping and the criterion to combine the seismic and aerodynamic loads were emphasized in these researches. In terms of the combination criterion, the square root of the sum of the squares (SRSS) method recommended by IEC 61400–1 [1] was found to underestimate or overestimate the combined seismic and aerodynamic loads and the linear combination method with a 0.75 combination factor was proved to be more accurate (see Prowell [31]), which is also adopted in ASCE-AWEA RP2011 [29]. However, later research proved that the SRSS method provides reasonably accurate results (see Santangelo et al., 2018[9]). This discrepancy implies that further investigation is needed for the combination criterion of the seismic and aerodynamic loads. A typical damping ratio of 5% including a 1% structural damping and a 4% aerodynamic damping was recommended by Witcher [21], Valamanesh and Myers [30] and ASCE-AWEA RP [29]. It is stated that no optimal aerodynamic damping exists and the typical damping ratio of 5% provides reasonable results by Santangelo et al., 2016 [6] and Santangelo et al. [9]. Therefore, the accurate prediction of aerodynamic damping is also needed since it affects the accuracy of the combination criterion.

In this study the combined seismic and aerodynamic loads on the wind turbine support structures is systematically investigated by means of the coupled and uncoupled analysis approaches. The coupled analysis is performed using the aero-elastic model, which is multibody and finite element model (MBD-FEM) and much complicated than the standard lumped mass model used in the uncoupled analysis. Hence, the superposition principle is not satisfied for the structure such as wind turbines and better combination criteria are investigated. This study focuses on the combination criterion of uncoupled analyses considering the misalignment effect between wind and earthquake as the modeling approach of aerodynamic damping has been well addressed in Valamanesh and Myers [30].

The numerical models including the aero-elastic model of wind turbine, the finite element model of wind turbine, the way to generate earthquake waves and the way to determine the parameters in sway-rocking model are described in Section 2. The combined seismic and aerodynamic loads are predicted by the coupled analysis approach in Section 3 to investigate the angle effect. The criterion to combine the seismic and aerodynamic loads are investigated in Section 4 for the uncoupled analysis approach. Conclusions are given in Section 5.

Table 1
Summary of the MHI wind turbine.

Description	Value
Rated power	2.4 MW
Hub height (above MSL)	80 m
Rotor, hub diameter	92 m, 4.35 m
Tower diameter, thickness	3.00–4.00 m, 0.022–0.038 m
Nacelle and rotor mass	168,730 kg
Tower mass (with equipments)	360,000 kg
Mean sea level (MSL)	11.81 m
Substructure diameter, wall thickness	10–18 m, 0.154–3.8 m
Substructure height, oblique cone height	22 m, 11 m

Table 2
Summary of control parameters.

Rated power	2437 kW
Minimum generator speed	690 r/min
Rated generator speed	1150 r/min
Rated generator torque	21,087.7 Nm
Optimal torque control gain	0.556 N m/(rad/s2)
Torque control proportional gain	750.67
Torque control integral gain	170
Pitch control proportional gain	0.018884
Pitch control proportional gain	0.008226
Gain scheduling for pitch control	Yoshida (2011)

Table 3
Description of soil parameters.

Layer	Depth D (m)	Density ρ (t/m^3)	S-wave Velocity V_S (m/s)	P-wave Velocity V_P (m/s)	Soil type
Riprap	2.0	1.76	208	434	Sand
Naarai	72.0	1.76	370	1950	Sand
Bedrock	-	2.00	750	2850	Rock

2. Numerical models

The description of the aero-elastic model of the wind turbine is given in Section 2.1 and that of the finite element model is shown in Section 2.2. The way to generate the earthquake waves and the way to determine the stiffness and damping for the sway-rocking model are presented in Section 2.3 and Section 2.4, respectively.

2.1. The aero-elastic model of wind turbines

The wind turbine targeted in this study is a pitch-regulated MHI 2.4-MW wind turbine located at 3.1 km offshore Choshi, Japan (hereinafter as the MHI wind turbine). The outline of the MHI wind turbine and the soil profile supporting the gravity foundation are shown in Fig. 1. The information of the MHI wind turbine is summarized in Table 1. The aero-elastic code GH Bladed 4.8 [22] is adopted to build the wind turbine model, which can simulate the wind loads during the conditions of normal power production, idling or parking and emergency stop. The aerodynamic properties of the blade are based on the Japan Society of Civil Engineers (JSCE) guideline (Ishihara [32]). The variable blade-pith-to-feather control parameters are based on Yoshida [33], which are summarized in Table 2. The nacelle-yaw is not activated, and no yaw misalignment is assumed. The modal damping ratios of the first and second tower modes is determined as 0.2% according to the field measurements in Oh and Ishihara [34]. The soil parameters of Riprap layer are identified by Ishihara and Wang [35] and the whole soil parameters are described in Table 3. The foundation of wind turbine is built using the sway-rocking (SR) model and how to determine the spring stiffnesses and dashpot dampings will be described in Section 2.4. The validation of the aero-elastic wind turbine model can be found in Yamaguchi et al. [36]. The aero-elastic model can be found in Fig. 2(a).

2.2. The finite element model for wind turbines

The finite element model is necessary to predict the seismic loading in the uncoupled analysis. However, the finite element model needs to be verified by the aero-elastic model before its application. In this study, the three-dimensional (3D) finite element model called the standard lumped mass model (SLM, see its front view in Fig. 2b) is built for the targetted wind turbine and verified by the aero-elastic model (AEM, see Fig. 2a). In the SLM, the RNA, tower and substructure are modelled with the lumped masses and the Euler–Bernoulli beam elements. The gravity foundation is modeled by a lumped mass at the ground level and connected to the substructure base by using a rigid beam. The soil-structure interaction is modeled by the sway-rocking (SR) model at the ground level. According to the suggestion of JSCE 2010 [32], the number of tower beam elements is 24. All lumped masses and beam stiffnesses are determined according to the real wind turbine. The structural damping is modeled by the Rayleigh damping model and the structural damping ratios of the first and second modes are determined as 0.2%. During the

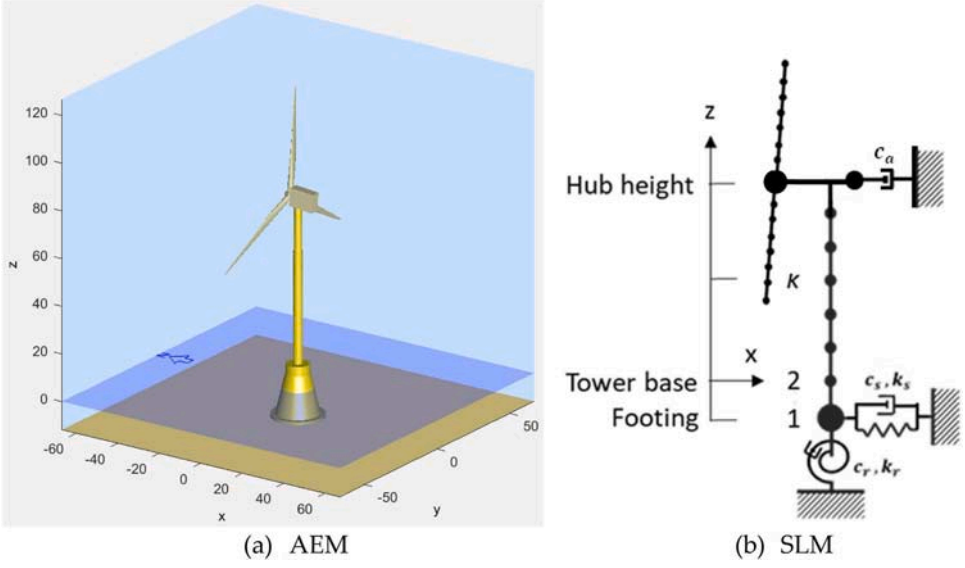

Fig. 2. AEM and SLM for the gravity foundation supported wind turbine.

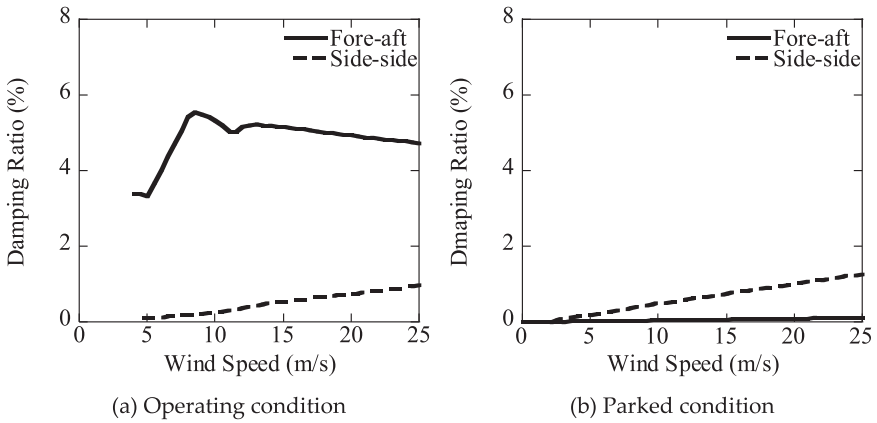

Fig. 3. Variation of aerodynamic damping ratio with wind speed.

Table 4
Numerical analysis scheme.

Dynamic analysis	Newmark-beta method ($\beta = 1/4$)
Eigenvalue analysis	Subspace iteration procedure
Element type	Beam element
Formulation	Total Lagrangian formulation
Structural damping	Rayleigh damping
Time interval	$\Delta T = 0.02s$
Integration time	$T_{\max} = 120s$

prediction of seismic loads, the aerodynamic damping is modelled by a dashpot at the hub height in the SLM. The method in Valamanesh and Myers [30] is used to determine the values of dashpots, from which the modal damping ratio of aerodyanmic damping ($\zeta = c_a/2m\omega$) can be obtained and shown in Fig. 3. The FE models with the seismic excitation are solved by the Newmark-beta method as summarized in Table 4.

Table 5 compares the modal frequencies obtained from the modal analysis for the aero-elastic model and the SLM model. It is noticed that the modal frequencies of the first three modes in the SLM model show good agreement with those in the aero-elastic model. Fig. 4 compares the modal shapes of the first three modes in two models. It is found that the modal shapes in the SLM model also match well with those in the aero-elastic model.

Since the modal frequencies obtained from the modal analysis in Bladed are for the uncoupled tower modes, a free decay analysis is designed to obtain the modal frequencies for the coupled tower mode for both normal operation and parked condition. A constant force is added on the tower top through the point loading function in the Bladed and lasts for 60 s. After that, the whole wind turbine behaves a free vibration, and the time-series of nacelle acceleration can be obtained, see Fig. 5(a). Finally, the modal frequency for the coupled tower mode can be extracted from the Fourier spectrum of the nacelle acceleration, see

Table 5
Comparison of modal frequencies of aero-elastic model and standard lumped mass model.

	Model	Fore-aft			Side-side		
		1st	2nd	3rd	1st	2nd	3rd
Frequency (Hz)	AEM	0.358	2.674	3.964	0.356	2.314	3.964
	SLM	0.360	2.960	3.777	0.356	2.278	3.931
Frequency ratio	f_{SLM}/f_{AEM}	1.01	1.10	0.953	1.0	0.984	0.992

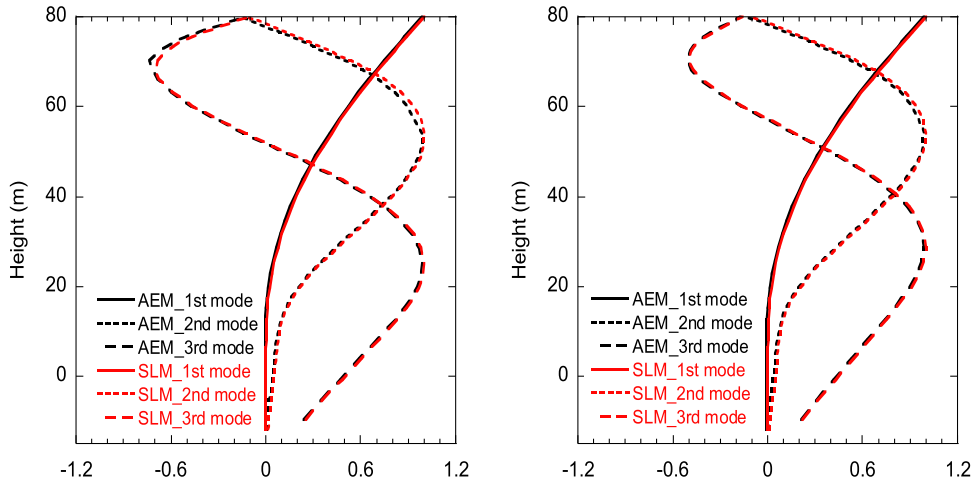

Fig. 4. Comparison of measured and predicted modal shapes by the identified soil parameters.

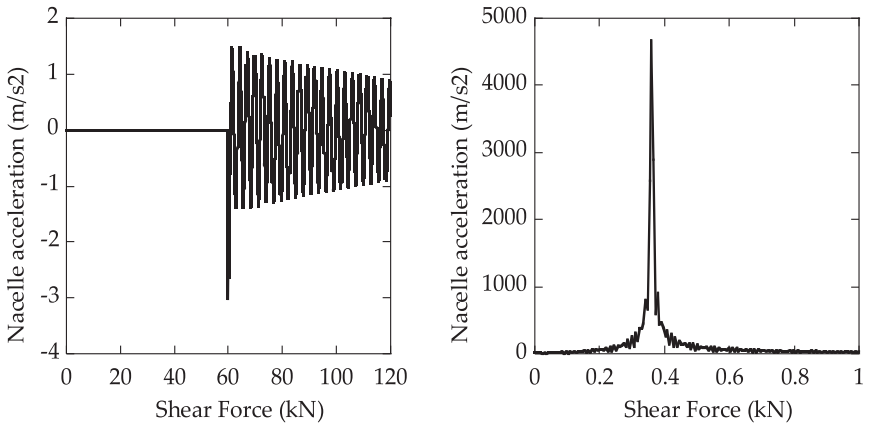

(a) Time-history of nacelle acceleration (b) Fourier spectrum of nacelle acceleration

Fig. 5. Time history and Fourier spectrum of nacelle acceleration.

Table 6
Comparison of modal frequencies in aero-elastic model and finite element model.

Operational scenario	Aero-elastic model (Hz)	SLM (Hz)
Normal operation	0.366 (FA & SS)	0.360 (FA); 0.363 (SS)
Parked condition	0.360(FA); 0.354 (SS)	0.360 (FA); 0.356 (SS)

Fig. 5(b). Table 6 compares the modal frequencies of the SLM to those of the coupled tower modes. It is found that the modal frequency for the normal operation is slightly larger than that of the parked condition, i.e., 3.4% error in the side-side direction, which is due to the rotational effect of rotor. In terms of the comparison of the SLM and the aero-elastic model, the SLM shows good agreement with the aero-elastic model for the parked condition when the Young's modulus of the nacelle beam is given as 2.05E+ 11 kPa. By increasing the Young's modulus of the nacelle beam to 2.05E+ 19 kPa, the SLM can agree better with the aero-elastic model for the normal operation (the error changes from 3.4% to 0.8% in the side-side direction).

To investigate the combined seismic and aerodynamic loads, the coordinate system to describe the wind turbine and the directions of earthquake and wind shall be determined in advance. As illustrated in Figs. 6(a)-6(b), the coordinate system is unique for the wind turbine supported by a centrosymmetric foundation such as the gravity foundation in this study. In this case, the fore-aft direction is taken the same as the x direction and the wind flow is thought to face to the rotor if the wind turbine is correctly yawed. Since an earthquake may occur along any direction relative to the wind turbine, the wind and earthquake may be not collinear. The angle between wind and earthquake is defined as θ. The values of θ between 0 degree to 90 degree shall be investigated for the combined wind and earthquake loads. In terms of the wind turbine supported by a non-centrosymmetric foundation such as the hexagon and the quadrilateral, the wind direction is not unique as shown in Fig. 5 (c). The angle between the wind direction and the X axis is defined as φ. For the circular section, only φ = 0 degree needs to be considered; for the hexagon section, φ = 0 degree and 30 degree needs to be

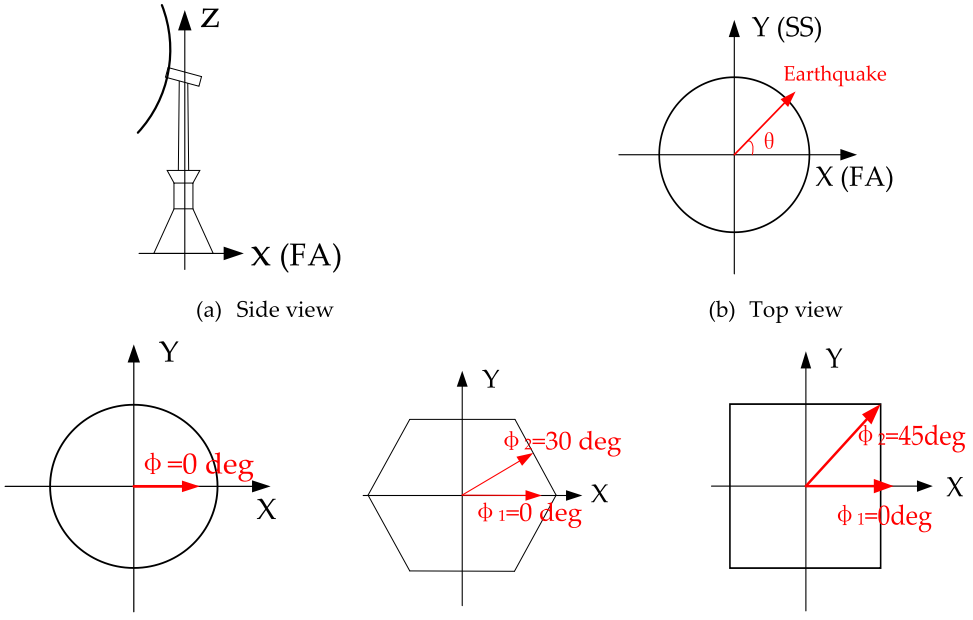

(a) Side view (b) Top view

(c) The definition of wind direction for various footing shapes

Fig. 6. The coordinate system and directions of wind and earthquake.

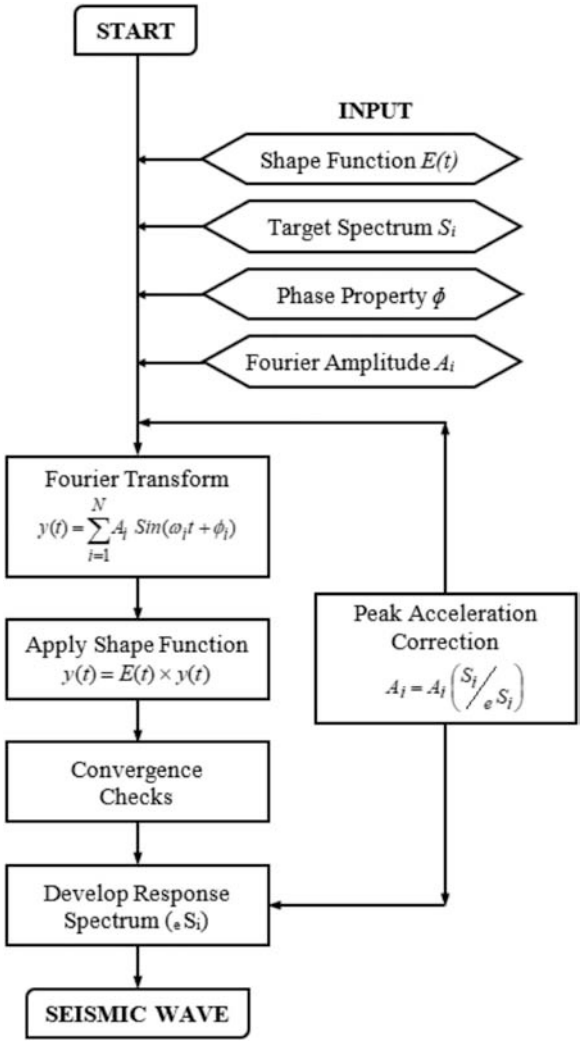

Fig. 7. Flow of iterative process for the generation of seismic waves with a targeted response spectrum [39].

investigated; for the quadrilateral section, φ = 0 degree and 45 degree needs to be investigated.

2.3. The generation of earthquake waves

As recommended in JSCE 2010 [32], the structural integrity and safety of wind turbine support structures are required against the level II earthquake with the recurrence period of 500 years. This also fulfills the requirement of the IEC 61400–1 guideline [1] which states that the ground acceleration corresponding to 475-year recurrence period should be considered for the seismic response evaluation of a wind turbine. For the level II earthquake, the response spectrum at the engineering bedrock is defined as follows:

$$S_{a_0}(T,0.05)=\begin{cases} a_0(1+9.375T)(0\le T\le 0.16) \\ 2.5a_0(0.16<T<0.64) \\ 1.6a_0/T(T\ge 0.64) \end{cases} \quad (1)$$

where $S_{a_0}(T,0.05)$ specifies the basic peak ground acceleration$a_0$at the engineering bedrock along with the frequency characteristic of the ground motions. a_0 is 3.2 m/s^2 for the level II earthquake and 1.6 m/s^2 for the level I earthquake; $T$is the natural period (s).

In this study, a synthetic accelerogram is generated based on the target spectrum described above, in which the phase characteristics of 4 typical real earthquake waves such as El Centro NS [37], Taft NS [37],

Table 7
Soil spring stiffness and damping value.

Stiffness in the sway direction K_S (N/m)	7.26E+ 9
Stiffness in the rocking direction K_R (Nm/rad)	6.80E+ 11
Damping in the sway direction C_S (Ns/m)	1.69E+ 8
Damping in the rocking direction C_R (Nms/rad)	3.83E+ 9

Table 8
Parameters for the normal operation.

Simulation software	GH Bladed 4.8
Wind condition	Rated wind speed of 11 m/s
Seismic condition	15 artificial Level II earthquake waves
Angle between wind and earthquake	0 degree; 45 degree; 90 degree

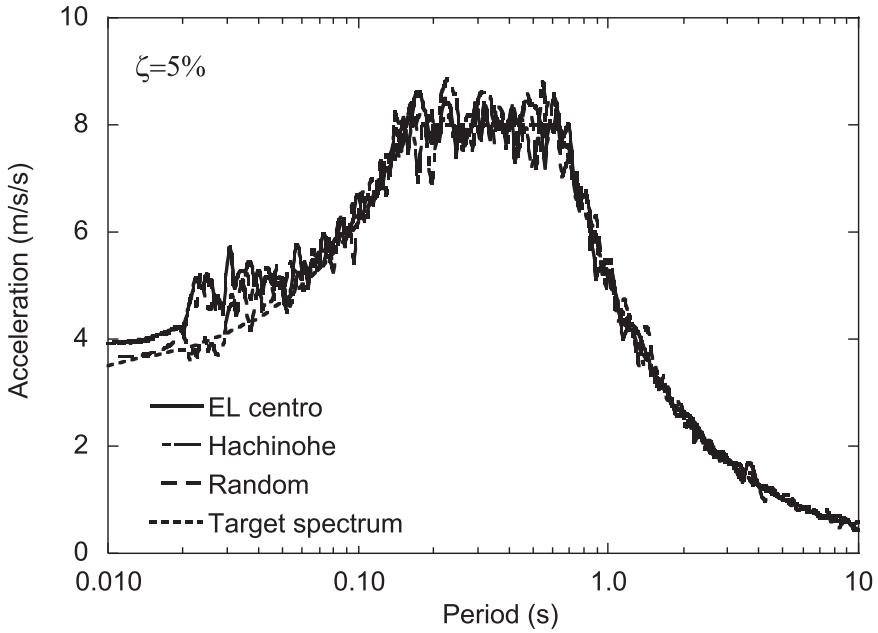

Fig. 8. Response spectra for the level II seismic waves with the damping ratio of 5%.

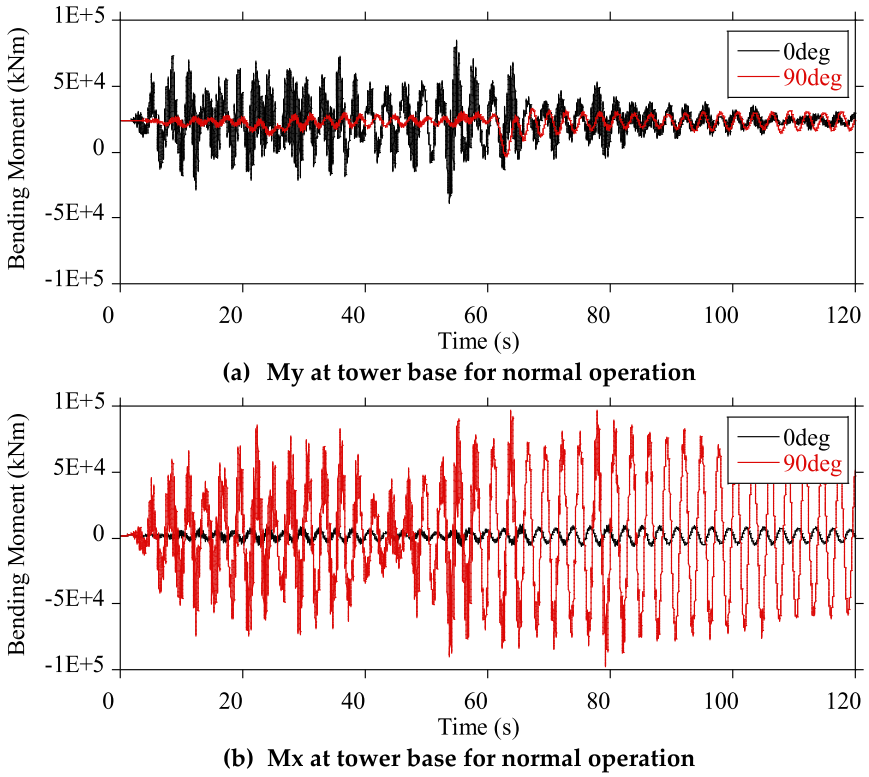

Fig. 9. Illustration of tower base moment for normal operation with two angles between wind and earthquake by the coupled analysis approach.

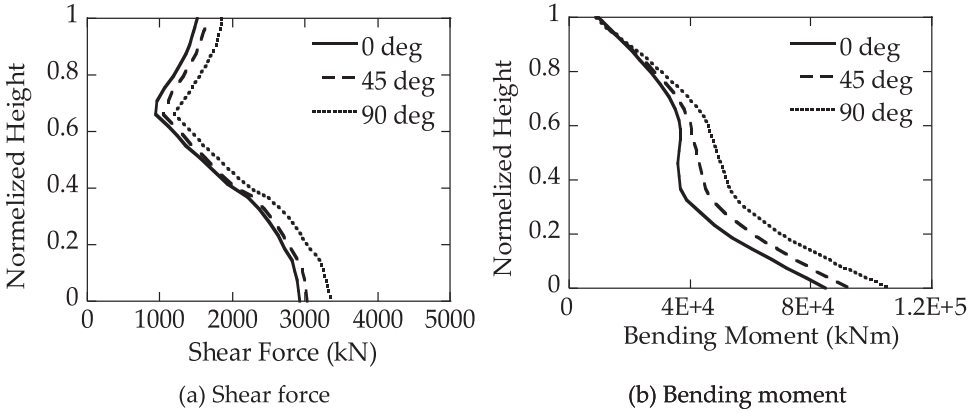

Fig. 10. Profiles of maximum combined loads for the normal operation with various angles between wind and earthquake by the coupled analysis approach.

Table 9
Shear force and bending moment at the tower base for various angles.

Angle between wind and earthquake	0 degree	45 degree	90 degree	Wind only
Shear Force (kN)	2931	3036	3361	354
Bending Moment (kNm)	85,017	92,375	105,893	23,850

Table 10
Parameters for the emergency stop.

Simulation software	GH Bladed 4.8
Wind condition	Wind speed from 11 m/s to 0 m/s
Seismic condition	15 artificial Level II earthquake waves
Angle between wind and earthquake	0 deg; 45 deg; 90 deg
Nacelle acceleration limit	300 gal; 250 gal; 200 gal
Pitch feathering rate	8 deg/s; 6 deg/s; 4 deg/s

Hachinohe EW [37], and JMA Kobe EW [38] and 11 random phase properties are used. Fig. 7 shows the flow chart for the generation of seismic waves (see Ishihara and Sarwar 2008[39]). Fig. 8 shows the response spectra of some generated earthquake waves with the damping ratio of 5%. Although the generated seismic waves are specified at the engineering bedrock, they are directly applied as the input for the aero-elastic and finite element models. This is because this study does not focus on the effect of the earthquake characteristics on the seismic loads of wind turbine supported structures. If it is needed, the seismic waves at the ground surface can be obtained by applying the equivalent linear soil dynamic analysis using the open-source software DYNEQ (see [40]).

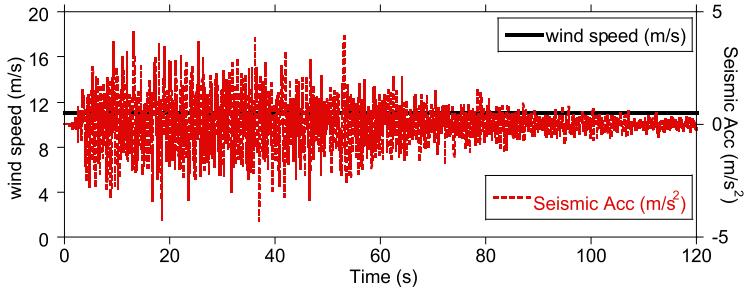

(a) Time history of wind speed and seismic wave

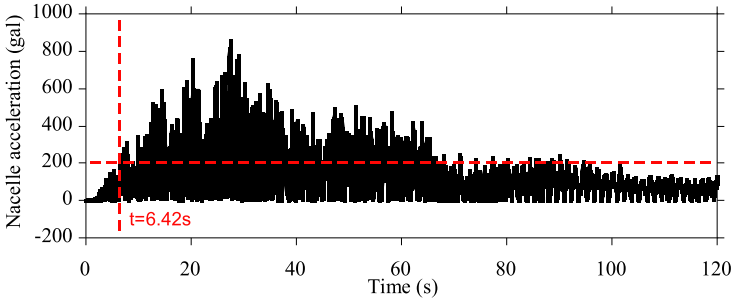

(b) Time history of nacelle acceleration

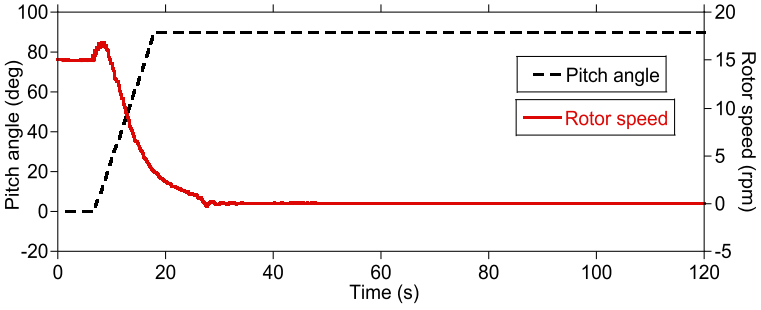

(c) Time history of pitch angle and rotor speed

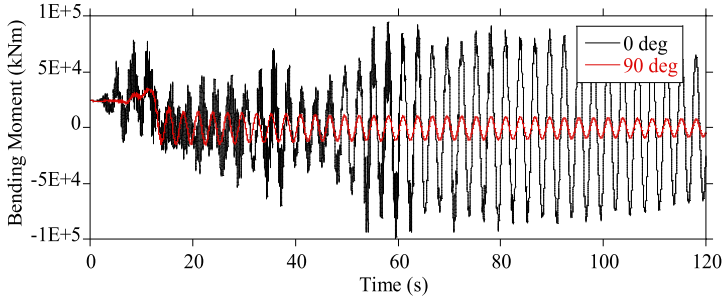

(d) My at tower base for emergency stop

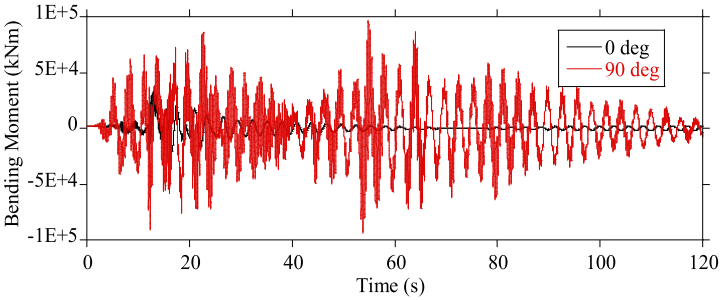

(e) Mx at tower base for emergency stop

Fig. 11. Illustrations of various time histories during the emergency stop.

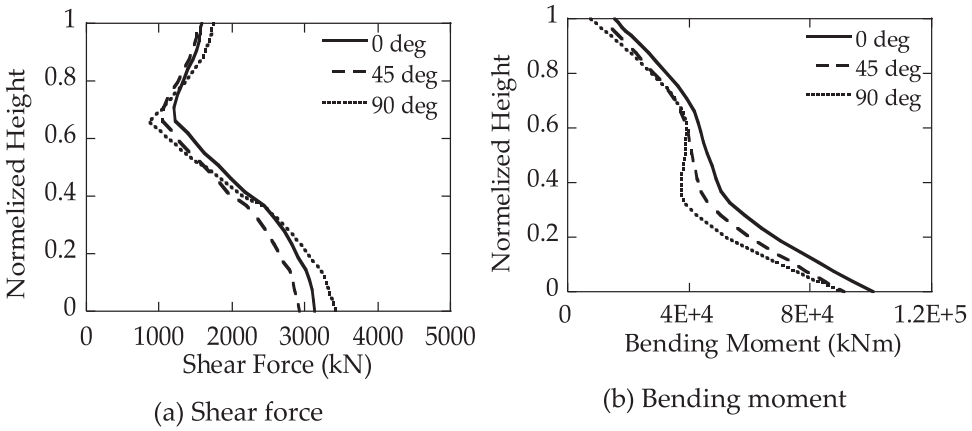

Fig. 12. Profiles of maximum combined loads for the emergency stop with various angles between wind and earthquake by the coupled analysis approach.

Table 11
Parameters for the parked condition.

Simulation software	GH Bladed 4.8
Wind condition	No wind (0 m/s) or cut-out wind speed (25 m/s)
Seismic condition	15 artificial Level II earthquake waves
Angle between wind and earthquake	0 deg; 45 deg; 90 deg

2.4. Parameters in sway-rocking model

Unlike the complicated soil-structure interaction models that are adopted in some previous researches (e.g. Santangelo et al. [6]), the equivalent linear sway-rocking model is adopted in this study. This is because the equivalent linear sway-rocking model can be easily achieved in both aero-elastic and FE models. Using the same soil-structure interaction model is a prerequisite to evaluate the agreement between the coupled and uncoupled analysis approaches. Since the soil-structure interaction is amplitude-dependent and frequency-dependent, the equivalent shear modulus and material damping of soil are adopted in this study and they can be obtained from the equivalent linear soil dynamic analysis. The values of spring stiffness and dashpot damping for the sway motion (K_S, C_S) and for the rocking motion (K_R, C_R) can be calculated by the Cone model with the equivalent soil parameters (see JSCE [32]). In terms of the monopile foundation supported wind turbine, an equivalent sway-rocking model can be derived from the Winkler model of the monopile foundation using the method in Ishihara and Wang [35]. Table 7 exemplifies the values of spring stiffness and dashpot damping for the targeted MHI 2.4-MW wind turbine.

3. Predictions of combined seismic and aerodynamic loads by the coupled analysis approach

According to the IEC61400–1 [1], the combined seismic and aerodynamic loads are investigated for the normal operation in Section 3.1, for the emergency stop in Section 3.2, for the parked condition in Section 3.3, respectively. After that, the various effects from the angle between wind and earthquake, the soil-structure interaction, the emergency stop conditions on the combined seismic and aerodynamic loads are discussed in Section 3.4.

3.1. Combined seismic and aerodynamic loads in the normal operation

The combined seismic and aerodynamic loads for the normal operation condition are evaluated with the parameters in Table 8. Note that since various wind speeds and earthquake waves were adopted in the previous researches (e.g. Asareh et al. [3], Santangelo et al. [6]), thousands of calculations were performed and a great many data were presented, which increases the difficulty for readers to catch the key points. To depict the results more effectively, only the rated wind speed is presented here since other wind speeds yield similar results and a statistical criterion is applied to address the combination of various earthquake waves (see Eqs.(2)–(3)). The misalignment effect on the combined seismic and aerodynamic loads is investigated for different operational scenarios. Three representative angles between wind and earthquake (that is, 0 degree, 45 degree and 90 degree) are picked up to illustrate the angle effect on the combined loads. The time-history of the resultant tower base moment for the cases of 0 degree and 90 degree are compared in Fig. 9. It is noticed that the total tower base moment for the case of 0 degree is much less than that of 90 degree. This is because larger aerodynamic damping exists in the case of 0 degree.

The combined shear force $Q_{i,j}(t)$ and bending moment $M_{i,j}(t)$ are estimated for the i^{th} angle and the j^{th} earthquake wave by Eq.(2). Correspondingly, the maximum shear force and moment are predicted by Eq.(3), which adopts the mean value of the maximum shear forces and bending moments predicted by 15 earthquake waves. Fig. 10 shows the maximum shear forces and bending moments on wind turbine tower in the normal operation. It is noticed that the maximum combined shear forces and bending moments increase along with the increase of angle and the maximum shear forces and moments occur in the case of 90 degree due to the small aerodynamic damping. The maximum shear force and bending moment at the tower base are also summarized in Table 9, in which the loads without earthquake are also added for comparison. It is found that the aerodynamic load only occupies 10.6%− 12.1% for shear force and 22.5%− 28.1% for bending moment, which means the seismic loads is dominant during the normal operation.

$$F_{i,j}(t) = \sqrt{F^2_{i,j,x}(t) + F^2_{i,j,y}(t)} \tag{2}$$

$$F_{\max\ ,i} = \frac{1}{N}\sum_{j=1}^{N}\left(\max\left(F_{i,j}(t)\right)\right) \tag{3}$$

Here, $i = 0, 45 or 90\text{deg}; j = 1, 2, ., N; N = 15$.

where $F_{i,j}(t)$ could be $Q_{i,j}(t)$ or $M_{i,j}(t)$ and $F_{\max\ ,i}$ represents the mean value of the maximum value of $F_{i,j}(t)$.

3.2. Combined seismic and aerodynamic loads in the emergency stop

The combined seismic and aerodynamic loads during the emergency stop are investigated using the coupled analysis with the parameters in Table 10, from which the effects of the nacelle acceleration limit and pitch feathering rate are investigated systematically with three different levels. Fig. 11 illustrates various time histories during the emergency

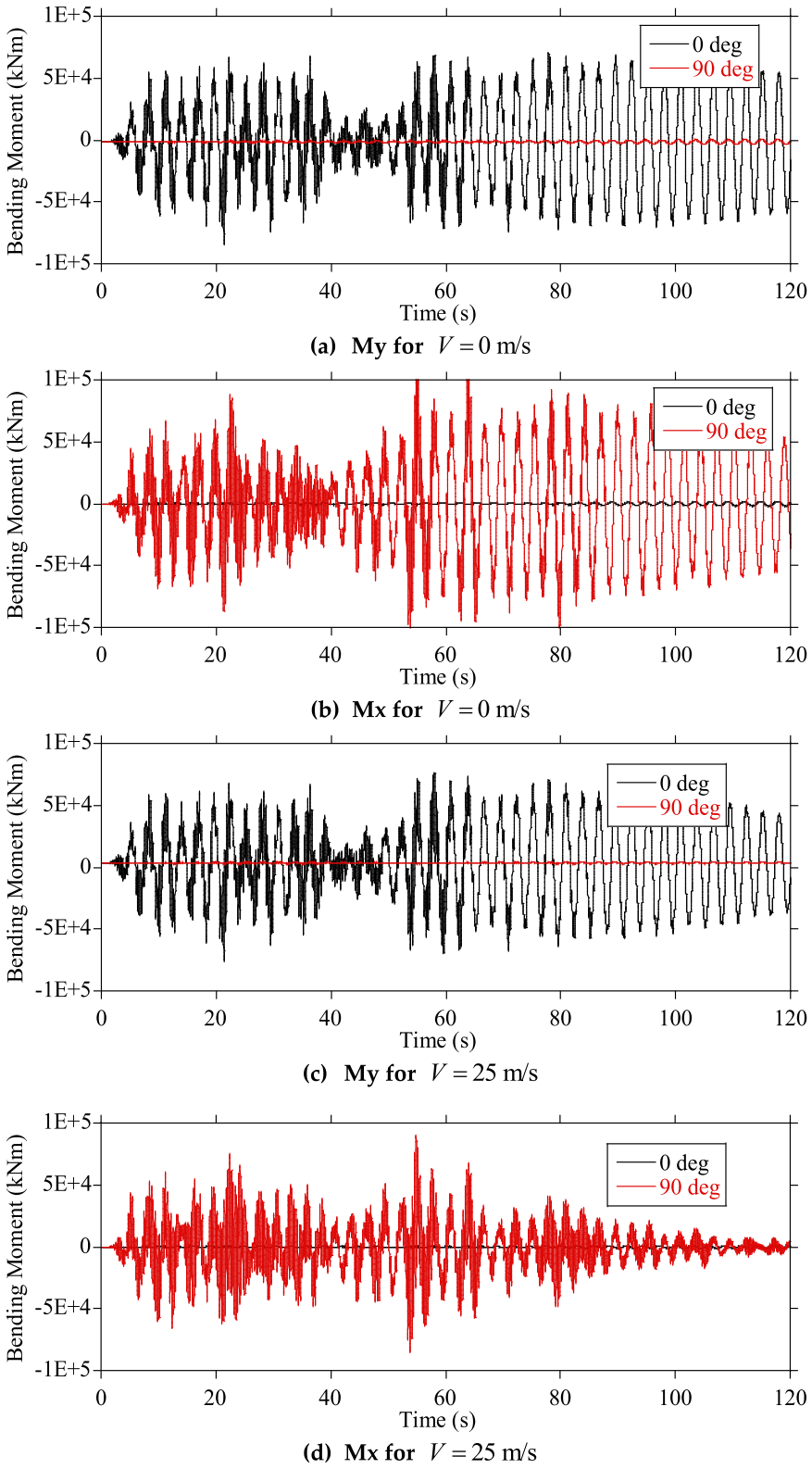

Fig. 13. Illustration of tower base moment for the parked condition with two angles between wind and earthquake by the coupled analysis approach.

stop with the nacelle acceleration limit of 200 gal and the pitch feathering rate of 8 degree per second for the case of 0 degree. It is noticed that the nacelle acceleration limit reaches 200 gal at 6.42 s, from which the emergency stops starts by feathering the blade pitch with the rate of 8 degree per second. The effects of the nacelle acceleration limit and the pitch feathering rate will be discussed in Section 3.4. The corresponding time histories of the tower base moment in X and Y directions are also illustrated in Fig. 10 for the cases of 0 degree and 90 degree. It is known that after the emergency stop occurs, the aerodynamic damping for X direction reduces to near zero while that for Y direction increases dramatically. Therefore, the moment in X direction shall be larger than that in Y direction. The maximum combined seismic and aerodynamic

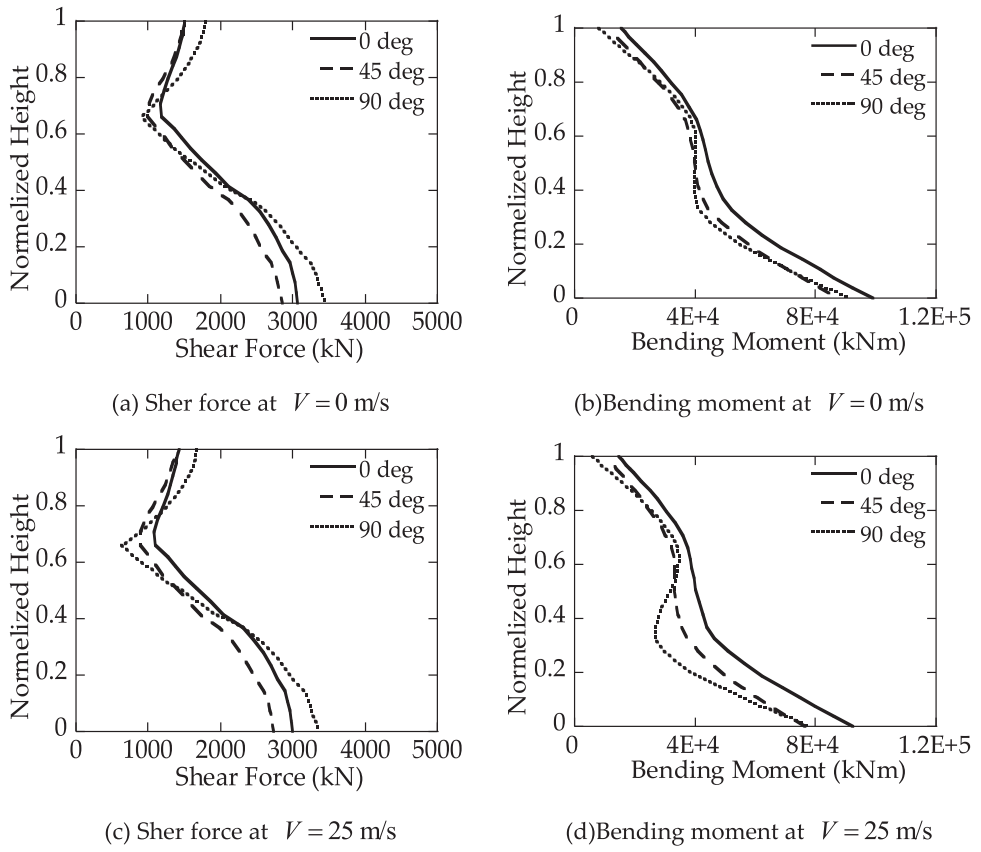

Fig. 14. Profiles of maximum combined loads for the parked condition with various angles between wind and earthquake by the coupled analysis approach.

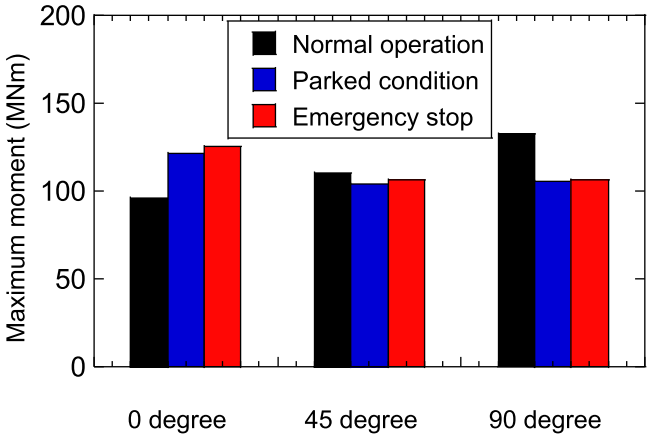

Fig. 15. The maximum tower base moments for different operational scenarios with various angles between wind and earthquake.

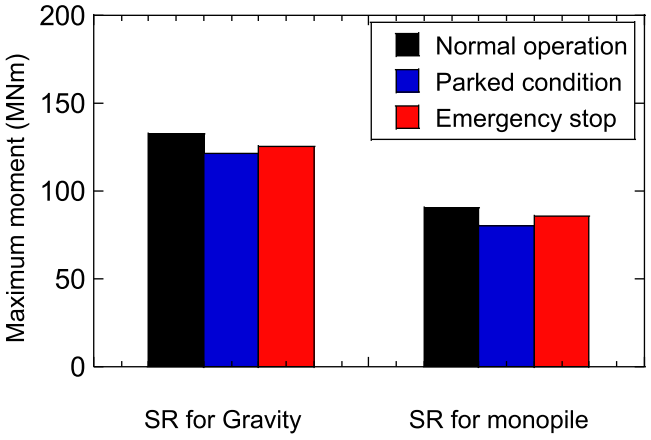

Fig. 16. The maximum tower base moments for different operational scenarios for wind turbine with different foundation types.

loads for the emergency stop are also predicted using Eqs.(2)–(3) and are presented in Fig. 12. It is found that the maximum bending moments of wind turbine tower for the case of 0 degree are larger than those for other cases.

3.3. Combined seismic and aerodynamic loads in the parked condition

Similarly, the combined seismic and aerodynamic loads in the parked condition are predicted with the parameters summarized in Table 11, in which two wind speeds including no wind ($V = 0$m/s) and cut-out wind speed ($V = 25$m/s) are considered. The predictions of the combined seismic and aerodynamic bending moments at the tower base are illustrated with the cases of 0 degree and 90 degree in Fig. 13. It is observed that for $V = 0$m/s, small difference exists between the bending moments corresponding to 0 degree and 90 degree while for $V = 25$m/s, significant difference exists between them. More specifically, the tower base moment for the case of 90 degree is smaller than that for the case of 0 degree for the wind speed of 25 m/s. These are caused by the difference of aerodynamic damping. For $V = 0$m/s, little aerodynamic damping exists for both cases of 0 degree and 90 degree while for $V = 25$m/s, little aerodynamic damping exists for the case of 0 degree but large aerodynamic damping exists for the case of 90 degree. The maximum combined loads for the parked condition are also predicted using Eqs.(2)–(3) and are presented in Fig. 14. It is found that the

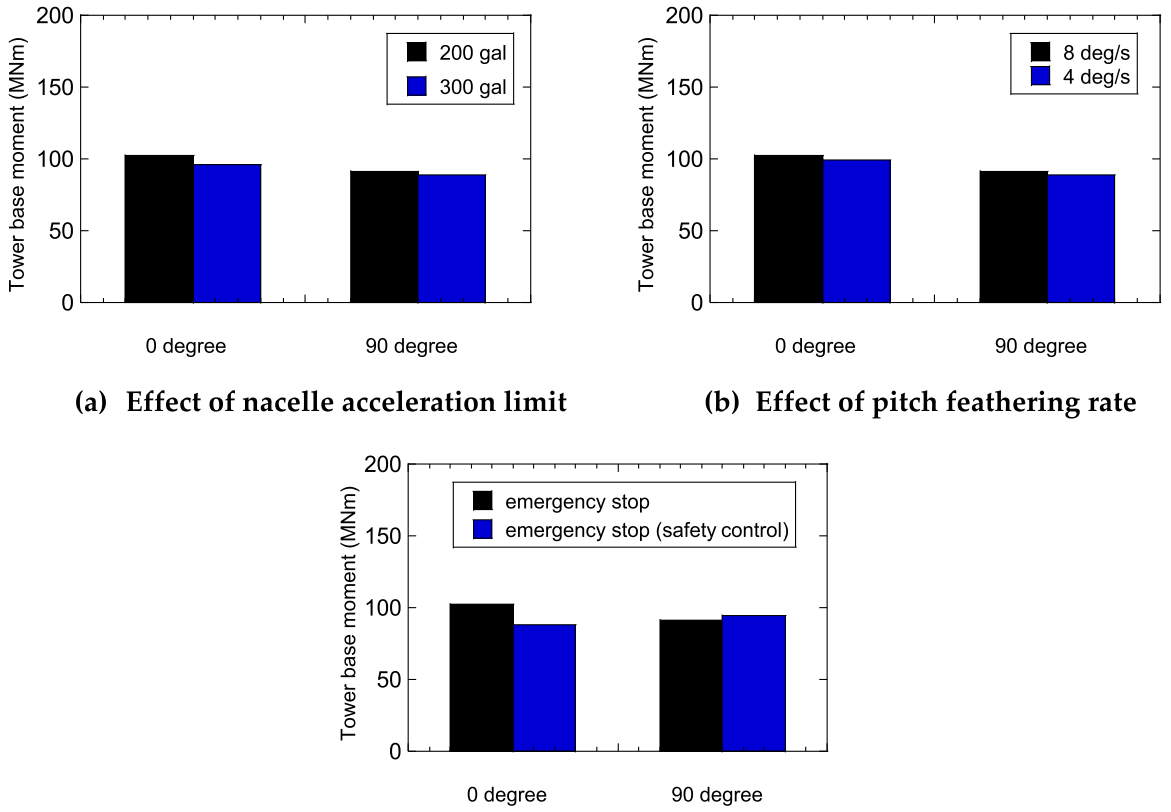

Fig. 17. Effects of nacelle acceleration limit, pitch feathering rate and activating safety system on the tower base moment for various angles between wind and earthquake.

maximum bending moment occurs at the case of 0 degree for both $V = 0\text{m/s}$ and $V = 25\text{m/s}$ due to the small aerodynamic damping. In addition, the bending moments for $V = 25\text{m/s}$ are smaller than those of $V = 0\text{m/s}$, which means the reduction of the combined seismic and aerodynamic bending moments by the aerodynamic damping exceeds the increase of the combined seismic and aerodynamic bending moments by high wind speed.

3.4. Various effects on the combined seismic and aerodynamic loads

The effect of the angle between wind and earthquake on the combined seismic and aerodynamic loads, which is referred as the angle effect, is summarized here. To quantify the scattering of combined seismic and aerodynamic loads caused by different phases in the 15 earthquake waves, a quantile of 85% is adopted and Eq. (3) can be replaced by Eq. (4) (see Kitahara and Ishihara [19]). Fig. 15 summarizes the combined tower base moments for different operational scenarios with various angles. It is noticed that for the cases of 0 degree, the emergency stop yields the maximum tower base moment, which is consistent with that in Witcher [19]. However, for the cases of 90 degree, the normal operation outputs the maximum tower base moment, which is consistent with that in Asareh et al. [3]. Therefore, the operational scenario that outputs the maximum combined seismic and aerodynamic loads varies along with the angle between wind and earthquake. However, the maximum combined loads can be pre-determined from the normal operation and emergency stop with the cases of 0 degree and 90 degree in the preliminary design.

$$F_{85} = F_{ave} + 1.04\sigma_F \tag{4}$$

where F_{85} could be Q_{85} or M_{85}. F_{ave} and σ_F are the mean value and standard deviation of the maximum value of $F_{ij}(t)$. Q and M represent shear force and bending moment, respectively.

Unlike this study for gravity foundation supported wind turbine, previous studies investigated combined seismic and aerodynamic loads more for monopile supported wind turbines, such as Witcher [21], Asareh et al. [3], Katsanos et al. [4], Yang et al. [5]. Hence, the influence of foundation type on combined loads is illustrated in Fig. 16 using the two foundation types. For each operational scenario of one certain foundation type, the maximum moment is selected for all misalignments between wind and earthquake. The 3 MW Vestas wind turbine is used here following Ishihara and Wang [35]. It is observed that the normal operation outputs the maximum combined loading for both foundations, which means the conclusion drawn from the angle effect suits different foundation types.

Fig. 17 summarized the effects of nacelle acceleration limit, pitch feathering rate and activating safety system on the tower base moment for various angles between wind and earthquake. It is noticed that these factors do have some effects on the tower base moment, which means that the optimal parameters and scenarios should be determined for certain wind turbines.

4. Predictions of combined seismic and aerodynamic loads by the uncoupled analysis approach

The uncoupled analysis approach to predict the combined seismic and aerodynamic loads is investigated in this section with the emphasis of the combination criterion for different operation scenarios in Sections 4.1–4.3.

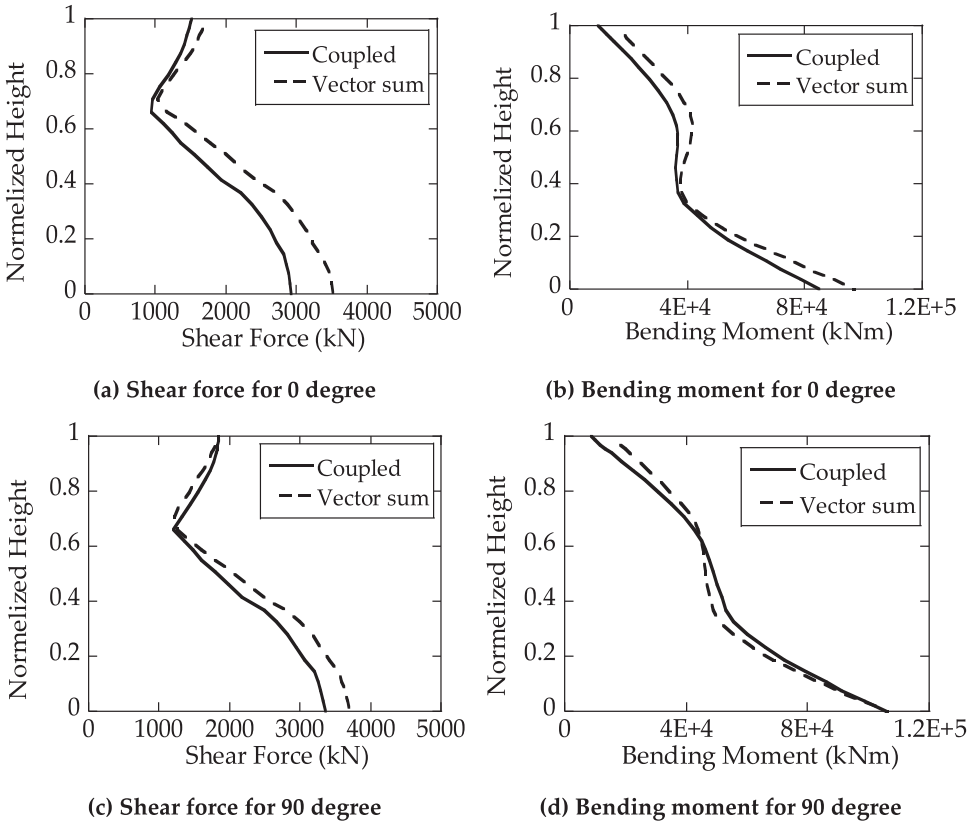

Fig. 18. Comparison of the profiles of combined seismic and aerodynamic loads by vector sum method and coupled analysis approach for normal operation.

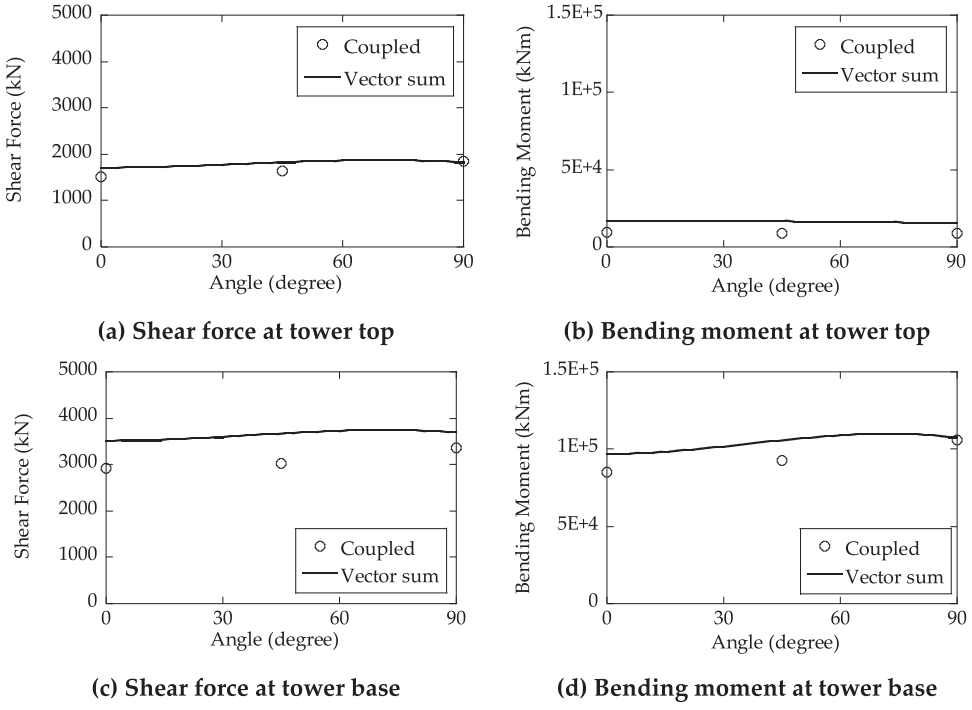

Fig. 19. Comparison of combined seismic and aerodynamic loads at tower top and base by the vector sum method and the coupled analysis approach for the normal operation.

4.1. Combination criterion for the normal operation

The vector sum method is proposed as the combination criterion to combine the seismic and aerodynamic loads for the normal operation in the uncoupled analysis approach, which is given as Eq.(5). The predicted combined seismic and aerodynamic loads by the coupled analysis approach with the parameters in Section 3.1 are utilized to verify the vector sum method. Fig. 18 illustrates the profiles of the combined shear

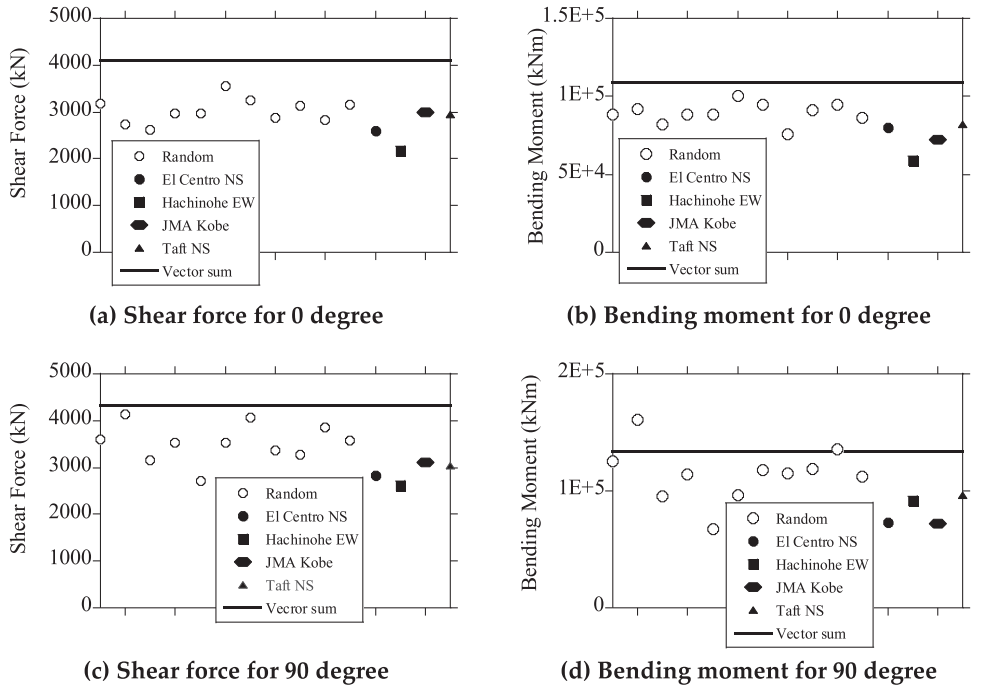

Fig. 20. Comparison of combined seismic and aerodynamic loads at the tower base with the quantile value of 85% by the vector sum method and the coupled analysis approach for the normal operation.

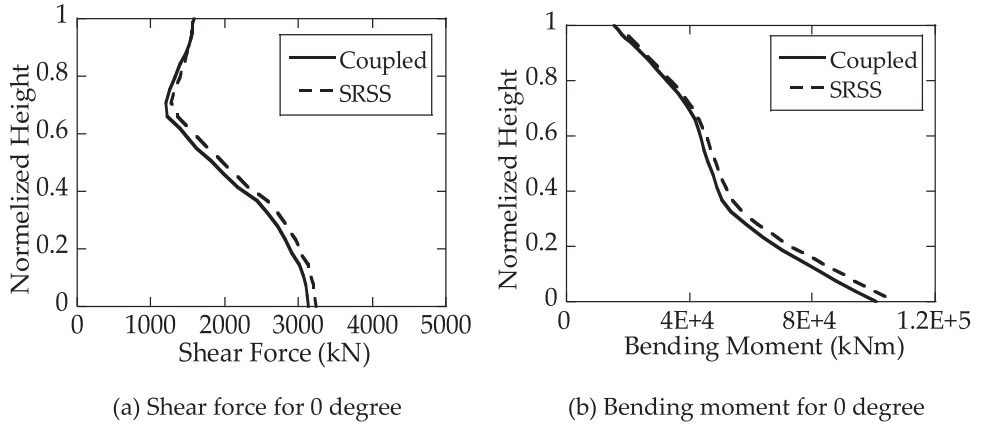

Fig. 21. Comparison of profiles of combined seismic and aerodynamic loads by the vector sum method and the coupled analysis approach for the emergency stop.

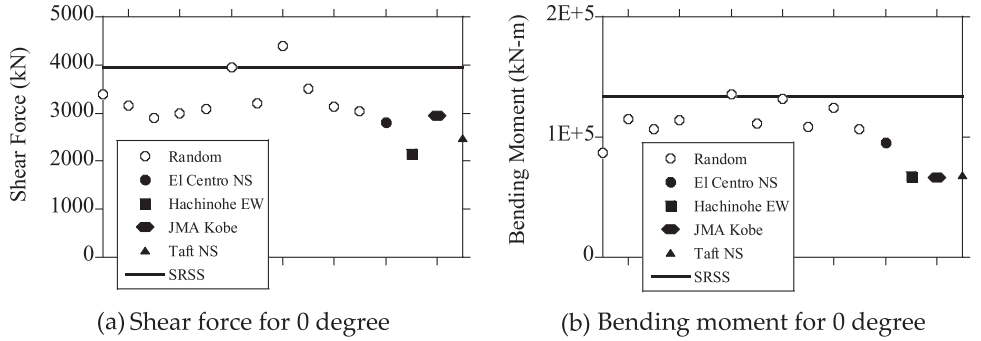

Fig. 22. Comparison of combined seismic and aerodynamic loads at the tower base with the quantile value of 85% by the SRSS method and the coupled analysis approach for the emergency stop.

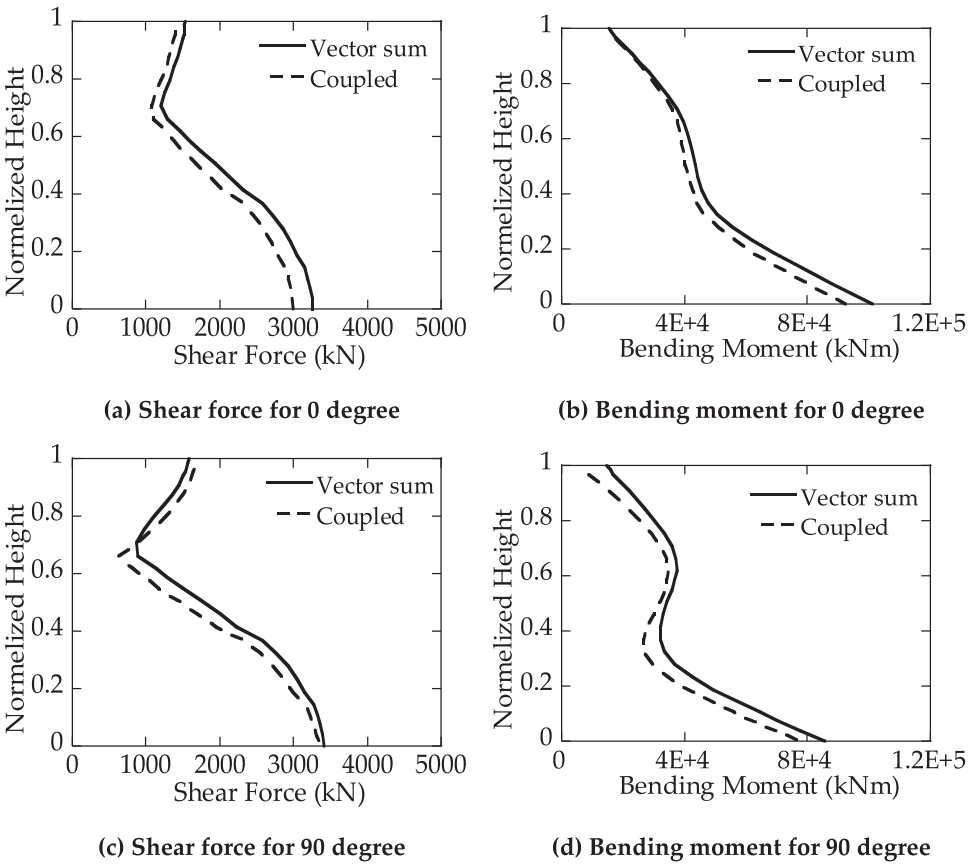

Fig. 23. Comparison of profiles of combined seismic and aerodynamic loads by the vector sum method and the coupled analysis approach for the parked condition.

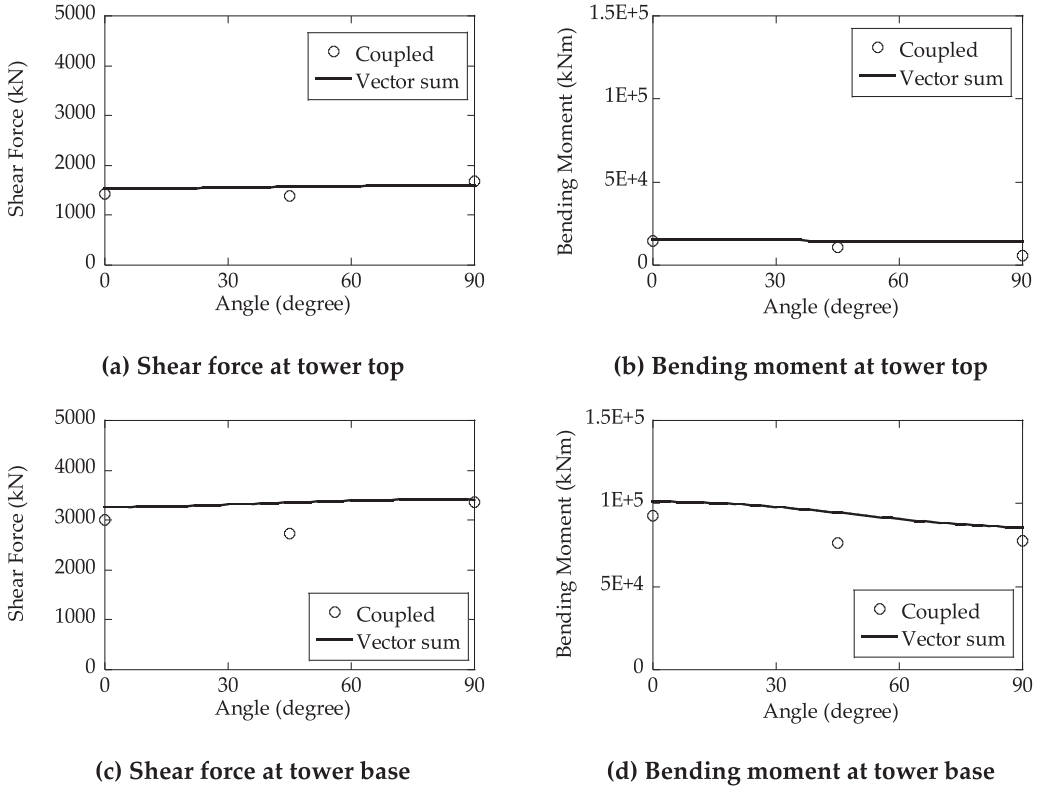

Fig. 24. Comparison of combined seismic and aerodynamic loads at the tower top and tower base for various angles between wind and earthquake by the vector sum method and the coupled analysis approach for the parked condition.

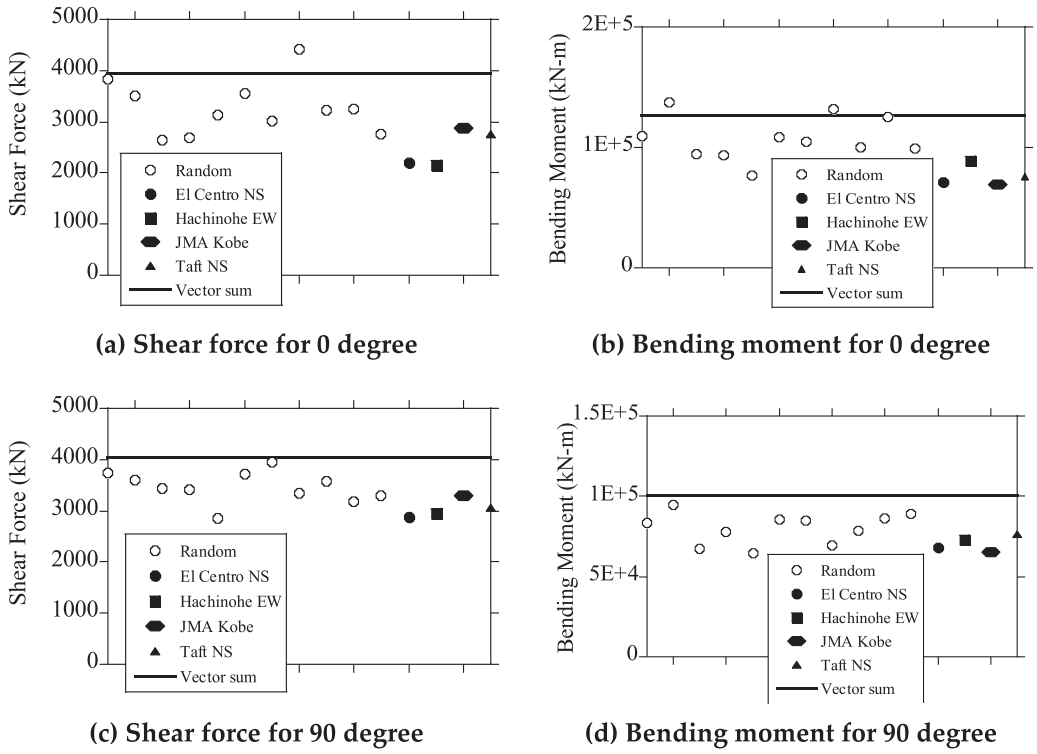

Fig. 25. Comparison of combined seismic and aerodynamic loads at the tower base with the quantile value of 85% by the vector sum method and the coupled analysis approach for the parked condition.

forces and bending moments for the cases of 0 degree and 90 degree. It is found that the predictions by the vector sum method reasonably cover those by the coupled analysis approach. To confirm the applicability of the vector sum method, Fig. 19 demonstrates the predicted combined seismic and aerodynamic loads at the tower top and tower base for various angles between wind and earthquake. For comparison, the results of linear sum method are also added in Fig. 19. It is observed that the vector sum method shows good agreement with the coupled analysis for both tower top and tower base while the linear sum method highly overestimates them. Note that the mean value of the predicted loads under 15 earthquakes waves are used in Figs. 19–20. To quantify the scattering effect, the quantile of 85% is adopted to address the predictions by the vector sum method, which is compared with all the predictions of 15 earthquake waves by the coupled analysis in Fig. 20. It is noticed that the predictions by the vector sum method with the quantile of 85% reasonably cover those predicted by the coupled analysis. Therefore, the vector sum method is verified for the normal operation systematically.

$$F_i = \sqrt{\left(F_{S,i}\cos\theta + F_{W,i}\right)^2 + \left(F_{S,i}\sin\theta + F'_{W,i}\right)^2} \tag{5}$$

whereF_i is the combined loads at the i^{th}height and Fcould be the shear force or the bending moment; $F_{S,i}$represents the maximum seismic loads; $F_{W,i}$ means the aerodynamic loads in the fore-aft direction while $F'_{W,i}$represents the aerodynamic loads in the side-side direction. The reason why$F'_{W,i}$ exists is that the rotor is not symmetrical in the side-side direction; θ is the angle between the seismic load and aerodynamic load.

4.2. Combination criterion for the emergency stop

The combination criterion for the emergency stop in the uncoupled analysis approach is determined as the square root of the sum of the squares (SRSS), which is shown in Eq. (6). The SRSS method is recommended in the IEC 61400–1 [1], which means it has been verified for the emergency stop in previous researches. In this study, the verification of SRSS method for the emergency stop is simplified. It is performed by applying the results of the coupled analyses for the case of 0 degree in Section 3.2. This is because that the case of 0 degree yields the maximum combined seismic and aerodynamic loads. The profiles of the combined shear forces and bending moments are depicted in Fig. 21 and the combined loads at the tower base with the quantile value of 85% by the SRSS method are portrayed in Fig. 22. It is noticed that the predictions by the SRSS method reasonably cover those by the coupled analysis approach. Therefore, the SRSS method is verified for the emergency stop. Note that the SRSS method is also verified for the cases of other degree, whose results are omitted for brevity.

$$F_i = \sqrt{\left(F_{ES,i}\right)^2 + \left(F_{S,i}\right)^2} \tag{6}$$

whereF_i is the combined loads at the i^{th}height and F could be the shear force or the bending moment; $F_{S,i}$ and $F_{ES,i}$ represent the maximum seismic loads and aerodynamic loads in emergency stop, respectively.

4.3. Combination criterion for the parked condition

The vector sum method shown in Eq. (5) can also be used as the combination criterion to combine the seismic and aerodynamic loads for the parked condition in the uncoupled analysis approach. The sum vector method is verified by the coupled analysis approach with the wind speed of $V = 25$ m/s in Section 3.3. Similar to those in Section 4.2, the profiles of the combined shear forces and bending moments for the cases of 0 degree and 90 degree are depicted in Fig. 23, the predicted combined seismic and aerodynamic loads at the tower top and tower base for various angles between wind and earthquake are plotted in Fig. 24, and the combined loads at tower base with the quantile value of 85% by the vector sum method are portrayed in Fig. 25. It is observed that the predictions by the vector sum method reasonably cover those by the coupled analysis approach. Therefore, the vector sum method is verified for the parked condition systematically. Note that the vector sum method is also verified for the wind speed of $V = 0$ m/s, whose

results are omitted for brevity.

5. Conclusion

This paper systematically investigates the combined seismic and aerodynamic loads on wind turbine support structures by means of the coupled and uncoupled approaches, in which the effect of the angle between wind and earthquake and the combination criterion are thoroughly discussed. Some conclusions are summarized:

1. The standard lumped mass model with a distributed rotor model and a lumped dashpot at the hub height show good agreement with the aero-elastic model in terms of the modal frequencies and modal shapes, which can be used to predict the seismic loading in the uncoupled analysis.
2. The maximum bending moment of wind turbine tower varies along with the angle between wind and earthquake for each operational scenario. When the angle equals to 0 degree, the emergency stop yields the maximum tower base moment while when the angle reaches 90 degree, the normal operation outputs the maximum loads.
3. The vector sum method for the normal operation and parked conditions and the SRSS method for the emergency stop are proposed to combine the seismic and aerodynamic loads in the uncoupled analysis approach. The proposed combination criteria show reasonable agreement with the coupled analysis approach.

Declaration of Competing Interest

We declare that we do not have any commercial or associative interest that represents a conflict of interest in connection with the work submitted.

Acknowledgement

This research was carried out as part of a joint program funded by ClassNK, Shimizu Corporation, J-POWER, Toshiba Energy Systems & Solutions Corporation and MHI Vestas Offshore Wind Japan. The authors express their deepest gratitude to the concerned parties for their assistance during this study.

References

[1] IEC 61400-1. Wind turbine generator systems part 1, safety requirements. International Electrotechnical Commission; 2019.
[2] Katsanos EI, Thöns S, Georgakis C. Wind turbines and seismic hazard: a state-of-the-art review. Wind Energy 2016;19(11):2113–33.
[3] Asareh MA, Schonberg W, Volz J. Effects of seismic and aerodynamic load interaction on structural dynamic response of multi-megawatt utility scale horizontal axis wind turbines. Renew Energy 2016;86:49–58.
[4] Katsanos EI, Sanz AA, Georgakis CT, Thöns S. Multi-hazard response analysis of a 5MW offshore wind turbine. Procedia Eng 2017;199:3206–11.
[5] Yang Y, Ye K, Li C, Michailides C, Zhang W. Dynamic behavior of wind turbines influenced by aerodynamic damping and earthquake intensity. Wind Energy 2018;21(5):303–19.
[6] Santangelo F, Failla G, Santini A, Arena F. Time-domain uncoupled analyses for seismic assessment of land-based wind turbines. Eng Struct 2016;123:275–99.
[7] Avossa AM, Demartino C, Ricciardelli F. Assessment of the peak response of a 5MW HAWT under combined wind and seismic induced loads. Open Constr Build Technol J 2017;11(1).
[8] Mo R, Kang H, Li M, Zhao X. Seismic fragility analysis of monopile offshore wind turbines under different operational conditions. Energies 2017;10(7):1037.
[9] Santangelo F, Failla G, Arena F, Ruzzo C. On time-domain uncoupled analyses for offshore wind turbines under seismic loads. Bull Earthq Eng 2018;16(2):1007–40.
[10] Failla G, Santangelo F, Foti G, Scali F, Arena F. Response-spectrum uncoupled analyses for seismic assessment of offshore wind turbines. J Mar Sci Eng 2018;6(3):85.
[11] Zuo H, Bi K, Hao H. Dynamic analyses of operating offshore wind turbines including soil-structure interaction. Eng Struct 2018;157:42–62.
[12] Wang P, Zhao M, Du X, Liu J, Xu C. Wind, wave and earthquake responses of offshore wind turbine on monopile foundation in clay. Soil Dyn Earthq Eng 2018;113:47–57.
[13] Ju SH, Huang YC. Analyses of offshore wind turbine structures with soil-structure interaction under earthquakes. Ocean Eng 2019;187:106190.
[14] Fan J, Li Q, Zhang Y. Collapse analysis of wind turbine tower under the coupled effects of wind and near-field earthquake. Wind Energy 2019;22(3):407–19.
[15] Zuo H, Bi K, Hao H, Li C. Influence of earthquake ground motion modelling on the dynamic responses of offshore wind turbines. Soil Dyn Earthq Eng 2019;121:151–67.
[16] De Risi R, Bhattacharya S, Goda K. Seismic performance assessment of monopile-supported offshore wind turbines using unscaled natural earthquake records. Soil Dyn Earthq Eng 2018;109:154–72.
[17] Kaynia AM. Seismic considerations in design of offshore wind turbines. Soil Dyn Earthq Eng 2019;124:399–407.
[18] del Campo JO, Martín, Pozos-Estrada A. Multi-hazard fragility analysis for a wind turbine support structure: an application to the Southwest of Mexico. Eng Struct 2019:109929.
[19] Kitahara M, Ishihara T. Prediction of seismic loadings on wind turbine support structures by response spectrum method considering equivalent modal damping of support structures and reliability level. Wind Energy 2020:1–22.
[20] Wang L., Ishihara T. A study of the effects of foundation uplift on the seismic loading of wind turbine tower and gravity foundation using a new dynamic Winkler model. Engineering Structures, under revision.
[21] Witcher D. Seismic analysis of wind turbines in the time domain. Wind Energy 2005;8(1):81–91.
[22] Bladed for windows user manual. Bristol, UK: Garrad Hassan and Partners; 2000.
[23] Jonkman JM, Buhl ML. FAST user's guide. Golden: National Renewable Energy Laboratory; 2005.
[24] Larsen T.J., Hansen M.A., How 2 HAWC2, the user's manual, Risø National Laboratory. Roskilde, Denmark: Technical University of Denmark, Technical Report Risø-R-1597 (ver. 4–5) (EN); 2014.
[25] Prowell I, Veletzos M, Elgamal A, Restrepo J. Experimental and numerical seismic response of a 65 kW wind turbine. J Earthq Eng 2009;13(8):1172–90.
[26] Bazeos N, Hatzigeorgiou GD, Hondros ID, Karamaneas H, Karabalis DL, Beskos DE. seismic and stability analyses of a prototype wind turbine steel tower. Eng Struct 2002;24(8):1015–25.
[27] Zhao X, Maißer P. Seismic response analysis of wind turbine towers including soil-structure interaction. Proc Inst Mech Eng, Part K J Multi-Body Dyn 2006;220(1):53–61.
[28] Umar Ahad B, Ishihara T. Seismic load evaluation of wind turbine support structures considering low structural damping and soil structure interaction. Eur Wind Energy Assoc Annu Event 2012:16–9.
[29] American wind energy assiciation. Recommended Practice for Compliance of Large Land based Wind Turbine Support Structures. ASCE; 2011.
[30] Valamanesh V, Myers AT. Aerodynamic damping and seismic response of horizontal axis wind turbine towers. J Struct Eng 2014;140(11):04014090.
[31] Prowell. An experimental and numerical study of wind turbine seismic behavior. San Diego: University of California; 2011.
[32] Ishihara T. Ed. Guidelines for Design of Wind Turbine Support Structures and Foundations (In Japanese); 2010.
[33] YOSHDA S. Variable speed-variable pitch controllers for aero-servo-elastic simulations of wind turbine support structures. J Fluid Sci Technol 2011;6(3):300–12.
[34] Oh S, Ishihara T. Structural parameter identification of a 2.4 MW bottom fixed wind turbine by excitation test using active mass damper. Wind Energy 2018;21(11):1232–8.
[35] Ishihara T, Wang L. A study of modal damping for offshore wind turbines considering soil properties and foundation types. Wind Energy 2019;22(12):1760–78.
[36] Yamaguchi Atsushi. Extreme load estimation of the wind turbine tower during power production. Wind Eng 2019. 0309524×19872766.
[37] Building Performance Standardization Association. Typical observed seismic waves (acceleration data). (In Japanese). Available from: http://www.seinokyo.jp/jsh/top/
[38] Japan Meteorological Agency. Strong seismic waveform (the 1995 Southern Hyogo Prefecture Earthquake). (In Japanese).
[39] Ishihara T., Sarwar M.W. Numerical and theoretical study on seismic response of wind turbines. In: European wind energy conference and exhibition; 2008. p. 1–5.
[40] Yoshida N, Suetomi I. DYNEQ: a computer program for dynamic analysis of level ground based on equivalent linear method. Reports of Engineering Research Institute. Sato Kogyo Co., Ltd; 1996. p. 61–70.